Effects of 1-pyrrolidinedithiocarbamate and 2,5-dimercapto-1,3,4-thiadiazole on lead corrosion behavior in chloride medium

W. Qafsaoui[a,*], A. Et Taouil[b], T.T.M. Tran[c], H. Cachet[c], S. Joiret[c]

[a] Faculté des Sciences d'El Jadida, Université Chouaïb Doukkali, BP 20, 24000 El Jadida, Morocco. wqafsaoui@gmail.com

[b] Institut UTINAM, UMR 6213 CNRS, Université de Franche-Comté, 30 Avenue de l'Observatoire, 25009 Besançon Cedex, France. abdeslam.et_taouil@univ-fcomte.fr

[c] Sorbonne Université, CNRS, Laboratoire Interfaces et Systèmes Electrochimiques, LISE, F-75005, Paris, France.

mai.tran_trong_long@sorbonne-universite.fr; hubert.cachet@upmc.fr; suzanne.joiret@upmc.fr

Abstract

The adsorption and corrosion protection of 1-pyrrolidinedithiocarbamate (PDTC) and 2,5-dimercapto-1,3,4-thiadiazole (DMTD) on bare Pb were investigated. Surface analyses revealed that for high concentration (*i.e* 10 mM), the organic molecules are strongly adsorbed on Pb surface. In 30 $g.L^{-1}$ NaCl, Pb corrosion current was highly decreased and anodic passivation was very efficient. EIS measurements and simulations enabled to evaluate organic films thickness, anodic charge transfer resistance R_{ta} and metal/film interface resistivity ρ_0. Efficient Pb corrosion protection was confirmed. Results obtained from Young and power law models showed that EIS parameters are not much dependent on the chosen analytical expression.

Keywords: *Organic coatings, Polarization, EIS, Surface characterization, Neutral inhibition*

1. Introduction

Most of research articles dealing with electrochemistry of Pb and its alloys mainly concern applications including roofs or gutters [1], artistic materials [2], lead-acid batteries [3,4] and archeological artefacts [5]. Its use has been highly decreased for the past decades because of its toxicity when ingested [6]. Pb is very reactive with most environments. SO_2, CO_2 and carboxylic acids are the main species that lead to its degradation [7–9]. In some cases, its reactivity leads to its protection as when exposed to ambient atmosphere or buried in the ground, a protective film is spontaneously formed on the surface. It is mainly composed of Pb oxides (PbO) and of carbonate precipitates such as cerussite ($PbCO_3$), hydrocerussite ($Pb_3(CO_3)_2(OH)_2$) or plumbonacrite ($Pb_5(CO_3)_3O(OH)_2$) [7,10–14]. However, this spontaneous protection can be insufficient. For instance, when conserved in museums, Pb artefacts can be highly attacked by organic species (*e.g.* formic acid, acetic acid…) emitted through cellulose hydrolysis from wood materials in which they are stored [15]. Therefore, the need for preserving such ancient objects certainly motivates investigations of ways to limit as much as possible such degradation. Regardless of the final objective of the study, the interface Pb/environment is always of prime importance, especially the nature and properties of spontaneously grown layers on the surface which have a big impact on the Pb object's future use. In some cases, when exposed to aggressive medium, additional treatment on Pb must be carried out to increase lifetime of the metallic structure. Protection from Pb corrosion has been carried out through various ways. The application of thick deposits such as wax or acrylic coatings proved to be efficient [16] but they are not useful to conserve esthetic aspects of the material as they are too visible. Moreover, in the case of further attack, they are difficult to remove. The use of thin films, formed from corrosion inhibitors, has been more often carried out. Amino-organic and phosphoro-organic derivatives were shown to be

efficient toward Pb corrosion inhibition in acidic chloride solutions through stabilization of $PbCl_2$ protective layer [17,18]. Non-toxic compounds such as amino acids or saturated linear carboxylates have also been studied as corrosion inhibitors on Pb. Amino acids were shown to provide good protection against corrosion of Pb in neutral media, especially glutamic acid [19]. Carboxylates (*e.g.* decanoate) have been proved to provide Pb surface with good corrosion protection through formation of crystalline Pb carboxylate layer which exhibits good passivation properties [15,20,21]. More recently, innoxious dithio compounds such as 1-pyrrolidinedithiocarbamate (PDTC) and 2,5-dimercapto-1,3,4-thiadiazole (DMTD) have been successfully used as corrosion inhibitors on bronze in neutral solution [22,23]. In both cases, organic inhibitors' adsorption on bronze surface led to thick, insulating and protective layer enabling very good corrosion protection. Moreover, both PDTC and DMTD are efficiently adsorbed on Cu and Pb on bronze surface. Therefore, it seems interesting to study interactions between these molecules and bare pure Pb.

This paper investigates the interactions of Pb with PDTC and DMTD in neutral chloride medium. Spectroscopic techniques were used to study interactions of organic molecules on Pb and surface morphology was observed using scanning electron microscopy. Electrochemical experiments enabled to assess protective and insulating properties of grown organic films, especially through modeling of formed films' impedance with three different models: CPE (Constant Phase Element), Young and Power Law models.

2. Experimental and methods

2.1. Chemicals and materials

Chemicals were purchased from Sigma Aldrich® (analytical grade). Molecular structures of PDTC and DMTD are presented in Fig. 1.

The disk electrode was made of an allylic resin embedded 5 mm diameter cylinder rod of pure lead (Goodfellow, 99.999%). The electrode surface was polished on silicon carbide paper up to 1200 grade before rinsing thoroughly with deionized water.

FTIR analyzes were carried out on 1 cm² samples cut from a 3 mm thick lead sheet (Goodfellow, 99.95%).

2.2. Surface analyses

2.2.1. Scanning Electron Microscopy (SEM) / Energy Dispersive X-ray Spectroscopy (EDX)

A field emission gun scanning electron microscope (FEG-SEM, Zeiss, Ultra 55) coupled with energy-dispersive X-ray spectroscopy (EDX) was used to study surface morphology and composition. Element analyses were performed with a Quantax Bruker detector and data were analyzed by the Bruker Esprit software.

2.2.2. X-Fourier Transform Infrared Spectroscopy (FTIR)

Chemical composition of surface films was characterized using a Bruker VERTEX 70 FT-IR Spectrophotometer. Infrared absorbance spectra were recorded in the 600 - 2000 cm^{-1} range, with a resolution of 8 cm^{-1}. Before each sample scan, the signal of bare Pb substrate was taken as reference. Baseline correction was performed by OPUS 6.5 software after 200 scans of each sample.

2.3. Electrochemical measurements

Electrochemical measurements were carried out in aqueous solutions in a conventional three-electrode cell, using a Gamry potentiostat /galvanostat Model FAS-1 or 300C. The reference electrode was a saturated calomel electrode (SCE - E = 0.24 V/SHE at 25°C). The counter electrode was a platinum grid of a large surface area set close to the cell wall. The working

disk electrode was faced towards the cell bottom under stationary conditions without any stirring. For each experiment, 100 mL of electrolyte was used. Corrosion tests were carried out under temperature control (20°C) in 30 $g.L^{-1}$ NaCl naturally aerated solution.

2.3.1. Electrochemical polarization

Polarization measurements were performed after 1 hour immersion in the corrosion test solution (with or without PDTC or DMTD). Two independent measurements were carried out for each run: one from open circuit potential (OCP) towards cathodic potentials and the other from OCP towards anodic potentials (scan rate: 1 $mV.s^{-1}$).

2.3.2. Electrochemical impedance

The impedance measurements were performed applying 10 mV_{rms} from 100 kHz to 10 mHz (10 points per decade) at different immersion times up to 24 hours. Experiments were carried out at OCP. Zsimpwin™ and Simad softwares, the latter a lab-made software using a simplex regression method, were used to fit the data.

3. Results and discussion

3.1. Surface analysis

3.1.1. SEM and EDX analysis

Fig. 2 and Fig. 3 show SEM images and EDX spectra of Pb surface after 24 hours immersion in 30 $g.L^{-1}$ NaCl without (blank) or with PDTC or DMTD. SEM image and EDX spectrum (reference) of bare Pb surface are also presented.

Fig. 2a confirms that Pb is a soft metal, easily scratched during mechanical polishing. Moreover, different products can be formed on its surface, depending on atmospheric or aqueous composition [7,24–26]. The enlargement of the image clearly shows the presence of

needles-shaped crystals spread over the surface. This film is probably composed of small quantities of Pb carbonates and oxides since the corresponding EDX spectrum shows the presence of weak peaks of C and O (Fig. 3).

After 24 hours immersion of Pb electrode in the blank test solution (Fig. 2b), the surface is covered with a layer of corrosion products in the form of raveled scales. This surface is more oxidized than bare Pb and seems to present as much carbonate species (Fig. 3). These carbonates are formed during air exposition before surface analysis and not during immersion in NaCl solution [27].

Addition of 0.1 mM PDTC leads to formation of a thin surface film (Fig. 2c). Needles-shaped crystals are visible, like on bare Pb surface (Fig. 2a). EDX spectrum (not shown) is similar to the one obtained for the blank. On the other hand, when PDTC concentration is brought to 10 mM, a covering layer is visible on Pb surface (Fig 2d). Besides, a weak peak for N appears around 0.39 keV, which confirms the presence of PDTC on the surface (Fig. 3), as well as the peak for C signal, slightly more intense than the one obtained in the case of the blank.

About DMTD, immersion in 0.1 mM solution leads to corrosion products with the same spectrum as the blank. Nevertheless, surface morphology is different and cubic crystals are present on Pb surface (Fig. 2e). On the other hand, at 10 mM, the surface is covered with a homogeneous film, free of oxides (Fig. 3) and very different in appearance from the one formed at 0.1 mM, as it exhibits tubular crystals (Fig. 2f).

Similar results were observed with PDTC and DMTD on copper in previous works [28,29]. In these works, it was shown that sulfur reacts with the metal surface through chemical adsorption. In the present case, EDX cannot reveal S role in action process of PDTC or DMTD as energies of S and Pb are very close. However, presence of N after PDTC or DMTD immersion at 10 mM can be evidenced by EDX through a low intensity peak at 0.39 keV. The

organic molecules are most likely adsorbed on Pb surface, as evidenced for other N-containing organic molecules used as corrosion inhibitors on Pb [15,19,20,30,31].

3.1.2. FT-IR spectroscopy analysis

FT-IR spectroscopy was employed to analyze Pb surface modified with PDTC or DMTD molecules, at different concentrations. The spectra are presented in Fig. 4.

The results show that in absence or presence of 0.1 mM of PDTC, Pb surface gets covered with Pb carbonate species as proved by the presence of a large band at 1400 cm^{-1} on FT-IR spectrum [32]. As affirmed before, these carbonates are not formed during immersion in NaCl solution but during air exposition [27].

For 1 and 10 mM PDTC, the molecule is present on the surface as most of its characteristic bands are observed on FT-IR spectra. For PDTC molecule, the band at 1000 cm^{-1} is attributed to C-S band [33]. Despite the two C-S bonds, this band is not split as the bonds are equivalent as a result of conjugation process. For 1 and 10 mM signals, the same band is present meaning either that the molecules are just physisorbed on Pb surface, without any chemical bond between S and Pb, or that bidentate coordination of PDTC on Pb surface occurs through S atoms. It is not easy to categorically address this point as Pb-S band lies between 1000 and 1100 cm^{-1} and, unfortunately, this region cannot be exploited as it already presents signals for bare PDTC molecule. Moreover, the possibility of bonds between N and Pb can be addressed. Indeed, interactions between organic inhibitors containing N atoms and Pb though adsorption process and formation of insoluble complexes were revealed in the literature, especially in the case of amino acids used as corrosion inhibitors on Pb [19,30]. Ghasemi *et al.* explained that electron pairs of N atoms can be shared with Pb orbitals to form insoluble complexes that protect the surface against corrosion through chemical adsorption process [30]. In the case of PDTC, this phenomenon can be enhanced since N atom is directly bonded inside an aliphatic

ring which will lead to donating inductive effects of the aliphatic ring towards N atom and increase interactions with Pb^{2+} ions formed on Pb oxidized surface. Similar behavior was observed for proline adsorbed on Pb in previous studies [30].

For 0.1 mM DMTD, the molecule is not present on the surface in spite of much smaller carbonate signal at 1400 cm^{-1}, compared to blank, resulting from a slight screening effect of DMTD, hindering surface attack.

For 1 and 10 mM DMTD, the molecule is adsorbed on the surface. When compared to bare molecule, the signal is different which must result from chemical adsorption of DMTD on Pb surface. The band at 1050-1060 cm^{-1} is attributed to C-S bond [34]. After surface modification with 1 or 10 mM DMTD, a new band arises, appearing as a shouldering at 1040 cm^{-1} which corresponds to Pb-S bond [35]. Therefore, it seems that DMTD is chemically adsorbed on Pb surface through S-Pb bonds.

3.2. Electrochemical measurements

3.2.1. Potentiodynamic polarization

Anodic and cathodic electrochemical behavior of Pb electrode was investigated in 30 $g.L^{-1}$ NaCl without (blank) or with 10 mM PDTC or DMTD (Fig. 5).

In the blank solution, Pb electrode is reactive since both cathodic and anodic current densities show very high values even at low overvoltages. The surface film formed on Pb electrode during immersion in 30 $g.L^{-1}$ NaCl does not provide good protection. In this medium, Pb is mainly covered with native oxide PbO and lead chloride products [7,15,24–26].

The main anodic and cathodic reactions are respectively the oxidation of Pb into Pb^{2+} ions (Eq. 1) and the oxygen reduction reaction (ORR) (Eq. 2).

$$Pb \rightarrow Pb^{2+} + 2e^- \quad \text{(Eq. 1)}$$

$$O_2 + 2H_2O + 4e^- \rightarrow 4OH^- \quad \text{(Eq. 2)}$$

In the presence of PDTC or DMTD, polarization curves are quite different. Values of corrosion current densities (Table 1), obtained graphically by extrapolation of Tafel lines to corrosion potentials, are 5 10^{-7} A/cm² , 6 10^{-8} A/cm² and 5 10^{-8} A/cm² for the blank, DMTD and PDTC modified substrates, respectively. Therefore, corrosion current density is reduced of about one decade with DMTD and PDTC modification. This indicates that these molecules have an important protective effect against Pb corrosion in neutral chloride media. Efficiencies are 88 % and 90 % for DMTD and PDTC, respectively, according to the following relationship:

$$\tau = 100\,\frac{j^0_{corr} - j_{corr}}{j^0_{corr}} \qquad \text{(Eq. 3)}$$

where τ is the efficiency ratio and j^0_{corr} and j_{corr} denote corrosion current densities in the absence and in the presence of the organic compound, respectively.

Regarding cathodic potential scan, in the presence of PDTC or DMTD, the shape of the cathodic branch is the same as the one of the blank. However, current density is decreased (in absolute value) as reduction process is hindered by both PDTC and DMTD based layers. This clearly indicates the effect of both molecules on the kinetics of ORR. Moreover, for potentials more cathodic than -770 mV/ECS in the presence of PDTC and -570 mV/ECS for DMTD, a change in the slopes of cathodic branches is observed showing an increase in current density. The low current densities observed from E_{corr} until -770 mV/SCE for PDTC and -570 mV/SCE for DMTD result from the decrease in the number of ORR active sites through chemical and physical adsorption of PDTC and DMTD on Pb surface.

For anodic branches, current density remains very low over large potential ranges. These pseudo plateaus are consistent with passive behavior that may be mostly attributed to the protective insoluble PDTC and DMTD based complexes layer formed on Pb oxidized surface and to the physically adsorbed organic molecules blocking active sites of Pb, as suggested from surface analysis results.

The results obtained in this paragraph show that PDTC and DMTD affect the electrochemical oxygen reduction reaction on Pb surface in 30 $g.L^{-1}$ NaCl, but their effect is more substantial on anodic lead dissolution.

3.2.2. EIS measurements

EIS was used to follow surface film formation on Pb electrode in 30 $g.L^{-1}$ NaCl solution without (blank) or with 10 mM PDTC or DMTD. All measurements were performed at corrosion potential E_{corr} as a function of immersion time from 1 to 24 hours. Fig. 6a shows Nyquist plots and Fig 6b the corresponding Bode plots obtained after 12 hours of immersion at E_{corr}. Such behaviour was found typical of all impedance diagrams recorded at every selected immersion time. In any case, a capacitive loop is observed which cannot be accounted for with a single time constant. In fact, two contributions are expected due to surface film and to charge transfer. The diameter of this loop (Fig. 6a) is higher in the presence of PDTC and DMTD, showing better surface protection in the presence of these organic compounds. This is also observed with impedance modulus $|Z|$ (Fig. 6b), since the obtained value at low frequencies for the blank is lower than those measured with organic inhibitors. Bode diagram gives evidence of a complicated frequency dependence of the electrode impedance. Particularly in the presence of organic molecules, in log-log coordinates, Z modulus varies linearly with frequency over at least 3 decades, with a slope slightly lower than unity, characteristic of a CPE behavior, element to be considered further in the Z modelling.

EIS measurements were simulated by means of the equivalent electrical circuit depicted in Fig. 7 in the line of what has been already proposed in literature [36]. This model was retained as the simplest physical description of the response of a metal electrode covered by a film having both conductive and dielectric properties. The charge transfer is assumed to occur

through the film and, at corrosion potential, both anodic and cathodic transfer reactions must be taken into account *a priori*.

In this model, the solution resistance R_s lies in series with the parallel combination of a constant phase element (Q_f, n_f) representing the film impedance Z_f and a film resistance R_f in series with a transfer impedance Z_{tr}, accounting for both anodic and cathodic reactions. In the model, Z_{tr} is the parallel combination of the *a priori* non-ideal double layer capacitance Q_{dl} [37] with two branches formed by the series arrangement of a transfer resistance with a Warburg diffusion impedance (R_{ta}, W_a) and (R_{tc}, W_c) respectively.

Experimental spectra were analyzed according to the equivalent circuit of Fig. 7 using ®ZSimpWin software providing the optimal value for each circuit element associated with a confidence interval. Unlike the purely capacitive situation of a passive electrode studied in the work of Gharbi *et al*. [37], the non-ideality of the capacitive double layer response cannot be actually determined due to the presence of transfer reactions. Therefore, instead of a CPE element Q_{dl}, a pure capacitance C_{dl} was systematically used for all EIS spectra analysis. The uncertainty on the R_s, Q_f, n_f parameters was about 1-3%, 20% on R_f and C_{dl}, 1-3% on transfer resistances, 1-10% on Warburg elements. The CPE exponent of the film impedance was always higher than 0.9, not too far from ideal behaviour. The origin of its CPE character will be discussed later within the frame of 3D models proposed in literature [38,39]. The actual film capacitance C_f can be graphically evaluated as the high frequency limit of the complex capacitance C*(ω) [22,40], calculated from the measured impedance Z(w) corrected for the solution resistance, according to:

$$C^*(\omega) = \frac{1}{j\omega(Z(\omega) - R_s)} \qquad (4)$$

Variations of the most relevant parameters with immersion time are plotted in the following figures. In Fig. 8a, the film resistance R_f is found of the order of a few $\Omega.cm^2$ in the absence of organic additive and arises from a native and porous PbO layer. In the presence of PDTC or DMTD, R_f reaches about 10^4 $\Omega.cm^2$. Remarkably, after 10 hours of immersion, PDTC and DMTD give rise to the same film resistance. Fig. 8b shows variations of the film capacitance C_f markedly differentiated for the three systems. For the blank, assuming that only PbO is present on the surface, C_f shows a constant value of 2.4 $\mu F.cm^{-2}$ during the entire immersion period and is equivalent to a PbO layer of 10 nm thickness, taking ε =25.9 for its dielectric constant [41]. With DMTD, the value of C_f is equal to 1 $\mu F.cm^{-2}$, irrespectively of immersion time, leading to a 3-4 nm thick organic film, assuming a dielectric constant ε =4. With PDTC, the surface film is five times thicker, the thickness slightly increasing with immersion time. Note that the above values for surface layer thickness were evaluated by considering C_f as a plane capacitor of thickness d and dielectric constant ε, as:

$$d = \varepsilon\varepsilon_0 / C_f \qquad (5)$$

with $\varepsilon_0 = 8.84\ 10^{-12}$ F/m in MKSA units.

The distinction between anodic and cathodic charge transfer resistances was made on the basis of the current-voltage behaviour, indicating that the cathodic reaction is more active than the anodic one. Consequently, the lowest resistance values were assigned to the cathodic reaction and the highest ones to the anodic reaction.

Fig. 9a shows the evolution of anodic and cathodic charge transfer resistances for Pb electrode in the absence of organic additive. At the beginning, R_{ta} is about 2 $k\Omega.cm^2$ stabilizing at 10 $k\Omega.cm^2$ after formation of the oxide layer. R_{tc} is ranging in between 0.6 and 2 $k\Omega.cm^2$. As shown in Fig. 9b, when DMTD or PDTC are present, anodic transfer resistance R_{ta} is increased by almost two orders of magnitude demonstrating the protecting character of both

molecules against Pb dissolution. However, the highest R_{ta} values are obtained with PDTC meaning that PDTC is a more efficient Pb corrosion inhibitor than DMTD.

Let's note that if just one RW branch is put for the charge transfer impedance, the "double layer capacity" becomes a CPE element with a coefficient close to 0.5, which means no more information on the double layer capacitance and a problem of diffusion type. This has already been noted in previous studies [36]. The distinction between cathodic and anodic charge transfer impedances enables the separation of the double layer capacitive response while at the same time showing that part of the charge transfer is under diffusion control. This diffusion control can be explained by diffusion of reactants through porosity of the surface film. Therefore, use of a global charge transfer resistance was avoided in order to not formally include the diffusion effect into the CPE element, which should only represent the double layer capacity.

Fig. 10 shows the changes in double layer capacitance C_{dl} with immersion time. In all cases, a transient regime is observed for the first 5 hours of immersion, both for the blank surface film formation and for the films formed from interactions of organic molecules with Pb surface. Additionally, C_{dl} is a probe of the remaining free surface of Pb electrode, the lower the C_{dl} value, the larger the film surface coverage. Thus, for a very blocking film such as in the presence of organic molecules, C_{dl} shows very low values. However, in the case of the blank in which the oxide film is not as resistive and blocking, C_{dl} value is intermediate between the possible value for a bare electrode and the one for a totally blocked electrode. As for R_{ta}, the comparison at 20 hours of immersion has to be done with respect to the initial C_{dl} value for the Pb electrode before formation of the corrosion layer, *i.e.* 10 $\mu F.cm^{-2}$. The surface coverage of PDTC was $\theta = 0.999$ and of 0.990 for DMTD.

CPE behaviour analysis of the film impedance

As a first approach, the film impedance has been modelled by a CPE element (Q_f, n_f) pointing out a distribution of time constants. The latter can be related to a distribution of either dielectric or conductive properties of the superficial film along the dimension normal to the electrode surface. Classically, it is assumed that the non-ideal behaviour arises from a conductivity gradient between the metal/film and the film/solution interfaces. An analytical expression of the film impedance Z_{Young} was proposed in the literature [42–44] assuming that the resistivity ρ across the film varies exponentially with distance x as $\rho(x) = \rho(x=0)\exp(x/\delta)$ in which δ is a characteristic length shorter than the film thickness d. The dielectric properties are represented by a relative dielectric constant ε assumed to be the same across the film. The so-called Young impedance reads:

$$Z_{Young} = \frac{\delta/d}{j\omega C_f} \cdot Ln\left(\frac{1+j\omega\tau.exp(d/\delta)}{1+j\omega\tau}\right) \qquad (6)$$

In this expression, $C_f = \varepsilon\varepsilon_0 S/d$ is the film capacitance, S the geometric surface of the film and $\tau = \varepsilon\varepsilon_0\rho(x=0)$ is a time constant characteristic of the film, where $\rho(x=0)$ is the film resistivity at the film/solution interface and ω the angular frequency. ε and ε_0 are the relative permittivity of the film and the vacuum permittivity ($8.84\ 10^{-12}$ F/m), respectively. j is the imaginary number solution of $j^2 = -1$. The expression of Z_{Young} depends on three independent parameters δ/d, τ and C_f. However, it was shown in literature that the assumption of an exponential resistivity profile as proposed by Young does not result in low-frequency time-constant dispersion as it has to be for a CPE behaviour [38]. Another alternative approach to account for both resistivity gradient across a layer and CPE behaviour was to consider a power law profile [39]. The so-called power law model (PL) provides an analytical expression for the film impedance Z_{PL}:

$$Z_{PL} = g \frac{d\rho_d^{\frac{1}{\gamma}}}{(\rho_0^{-1} + j\omega\varepsilon\varepsilon_0)^{\frac{\gamma-1}{\gamma}}} \quad (7)$$

where d and ε have the same meaning as above, ρ_0 and ρ_d are the film resistivity at the metal/film and at the film/solution interfaces, respectively and g is a numerical function of γ defined as $g = 1 + 2.88.\gamma^{-2.375}$. γ is a constant related to the sharpness of the film resistivity variation. The expression of Z_{PL} depends on three independent parameters ρ_0, ρ_d and γ, providing a direct determination of the film resistivity. When using the PL model, the film capacitance C_f was determined from the complex capacitance representation, as explained before.

Contrary to the CPE representation, Z_{Young} and Z_{PL} expressions for the film impedance are not reducible to circuit elements hampering the use of the ZSimpWin software. Consequently, comparison between both film impedance models inserted in the scheme of Fig. 7 in place of CPE and experimental EIS data was performed using a non-linear fitting software developed at LISE laboratory (SIMAD). Confidence intervals for the fitted parameters were estimated empirically from the change in a single parameter value yielding an increase by a factor of 1.2 of the standard deviation characterising the fit quality, the other parameters staying fixed to their optimal value [45]. The values of the interfacial parameters taken out from the different fits are gathered in Table 2 for blank Pb electrode, Pb/DMTD and Pb/PDTC systems. Importantly, central parameter values and their uncertainties obtained with the CPE analysis as a reference are not significantly modified when CPE impedance was replaced by either Young or PL impedance. In particular, the transfer resistance for anodic corrosion reaction R_{ta} is well determined, in the range 1-5%, independently from the choice for the film impedance, conclusively proving the inhibiting character of DMTD or PDTC against Pb corrosion.

From the above discussion, it can be concluded that the relevant parameters of the impedance model are only slightly dependent on the analytical expression chosen for the surface film

impedance. Accordingly, it means that the variation of interfacial parameters with immersion time, as depicted in Fig. 6 to 11, is well representative of the actual behaviour of the immersed Pb electrode, without or with an organic additive.

Additional information from the power law model

By means of the PL model, it is possible to check the changes in the surface film resistivity as a function of immersion time. Fig. 11 shows the variations of the resistivity ρ_0 at the metal/film interface and ρ_d at the film/solution interface with immersion time for the blank electrode and in the presence of DMTD or PDTC. The uncertainty on ρ_d is very large, around 30-50%. Nevertheless, in the logarithmic representation, it can be stated that ρ_0 values (Fig. 11a) are always larger in the presence of an organic additive than for the blank electrode, indicating the insulating properties of organic films. Additionally, a high value of ρ_0 is reached as soon as the first hour of immersion for PDTC, due to its rapid adsorption process while it is more progressive for DMTD (after at least 12 hours of immersion). Considering ρ_d (Fig. 11b), the same trend is observed for PDTC (instantaneous) and DMTD (progressive). As the formed insoluble complex film does not possess electronic transport, the observed conductivity arises from ions penetration into the film. According to the PL model [39], the resistivity profile $\rho(x)$ is well approximated by the following expression: $\rho(x) = \rho_d.(x/d)^{-\gamma}$ with γ related to the CPE exponent n_f as $\gamma = (1-n_f)^{-1}$. It is found that for immersion times greater than 10 hours, the CPE exponent n_f stays around 0.93 ± 0.01 for almost all cases, except for DMTD for which it reaches 0.98. Assuming an increase of 10^{10} with respect to the resistivity ρ_d at the film/solution interface leads to estimate the spatial extension of the resistivity profile as 0.7.d for $n_f = 0.93$ and 0.4.d for $n_f = 0.98$. For the unprotected Pb electrode, there is a continuous increase in ρ_d with time, indicating a progressive densification of the blank surface layer.

4. Conclusion

The importance of concentration in organic inhibitors *i.e* 1-pyrrolidinedithiocarbamate (PDTC) and 2,5-dimercapto-1,3,4-thiadiazole (DMTD) was evidenced. The best corrosion protection on Pb was observed for the highest concentrations (10 mM) thanks to adsorbed organic layers blocking most of the electrode surface.

EIS measurements were simulated by a model having both conductive and dielectric properties. The film impedance has been modeled by a CPE element interpreted in terms of a resistivity gradient. In the presence of PTDC or DMTD, the film resistance R_f reaches 10^4 Ω.cm² instead of few Ω.cm² in the case of the blank. The film formed in the presence of DMTD was 3-4 nm thick while that of PDTC was more than 15 nm thick after 1h of immersion. Besides, the anodic charge transfer R_{ta} is highly increased demonstrating the protective character of the insoluble complexes layers against Pb dissolution.

The film impedance was also evaluated according to Young and power law models assuming that the non-ideal behavior is due to a conductivity gradient between the metal/film and the film solution interfaces. The results obtained show that the relevant parameters are not much dependent on the chosen analytical expression.

Moreover, a high value of the metal/film resistivity ρ_0 is reached fastly in the case of PDTC due to its rapid adsorption process on Pb surface. For DMTD, this process is more progressive. The same trend is observed for the resistivity ρ_d at the film/solution interface. The observed residual conductivity for these films arises from ions penetration into the film.

References

[1] L.L. Shreir, ed., Corrosion. 2: Corrosion control, 2. ed., repr, Newnes-Butterworth, London, 1979.

[2] S. Hecker, S. Bottinelli, eds., Lead in modern and contemporary art, Bloomsbury Visual Arts, London ; New York, 2021.

[3] D.A.J. Rand, Lead-acid batteries, J. Power Sources. 4 (1979) 252–255. https://doi.org/10.1016/0378-7753(79)85016-8.
[4] S.M. Caulder, A.C. Simon, Lead-Acid Battery Overview, in: D.W. Murphy, J. Broadhead, B.C.H. Steele (Eds.), Mater. Adv. Batter., Springer US, Boston, MA, 1980: pp. 199–203. https://doi.org/10.1007/978-1-4684-3851-2_9.
[5] R.H Brill, Lead and oxygen isotopes in ancient objects, Philos. Trans. R. Soc. Lond. Ser. Math. Phys. Sci. 269 (1970) 143–164. https://doi.org/10.1098/rsta.1970.0093.
[6] d'Henry A. Heck, M. Casanova, T.B. Starr, Formaldehyde Toxicity—New Understanding, Crit. Rev. Toxicol. 20 (1990) 397–426. https://doi.org/10.3109/10408449009029329.
[7] T.E. Graedel, Chemical Mechanisms for the Atmospheric Corrosion of Lead, J. Electrochem. Soc. 141 (1994) 922–927. https://doi.org/10.1149/1.2054858.
[8] B. Wehrli, E. Wieland, G. Furrer, Chemical mechanisms in the dissolution kinetics of minerals; the aspect of active sites: Dedicated to Werner Stumm for his 65th birthday, Aquat. Sci. 52 (1990) 3–31. https://doi.org/10.1007/BF00878239.
[9] W. Stumm, R. Wollast, Coordination chemistry of weathering: Kinetics of the surface-controlled dissolution of oxide minerals, Rev. Geophys. 28 (1990) 53. https://doi.org/10.1029/RG028i001p00053.
[10] V. Brusic, D.D. DiMilia, R. MacInnes, Corrosion of Lead, Tin, and Their Alloys, CORROSION. 47 (1991) 509–518. https://doi.org/10.5006/1.3585286.
[11] E.A. Joerg, O.F. Devereux, Electrochemistry of Lead in Simulated Ground Water Environments, CORROSION. 52 (1996) 953–957. https://doi.org/10.5006/1.3292089.
[12] E.E. Abd El Aal, S. Abd El Wanees, A. Abd El Aal, Anodic behaviour and passivation of a lead electrode in sodium carbonate solutions, J. Mater. Sci. 28 (1993) 2607–2614. https://doi.org/10.1007/BF00356195.
[13] R.M. Hozalski, E. Esbri-Amador, C.F. Chen, Comparison of stannous chloride and phosphate for lead corrosion control, J. - Am. Water Works Assoc. 97 (2005) 89–103. https://doi.org/10.1002/j.1551-8833.2005.tb10847.x.
[14] Y. Xie, D.E. Giammar, Effects of flow and water chemistry on lead release rates from pipe scales, Water Res. 45 (2011) 6525–6534. https://doi.org/10.1016/j.watres.2011.09.050.
[15] E. Rocca, C. Rapin, F. Mirambet, Inhibition treatment of the corrosion of lead artefacts in atmospheric conditions and by acetic acid vapour: use of sodium decanoate, Corros. Sci. 46 (2004) 653–665. https://doi.org/10.1016/S0010-938X(03)00175-6.
[16] V. Costa, F. Urban, Lead and its alloys: metallurgy, deterioration and conservation, Stud. Conserv. 50 (2005) 48–62. https://doi.org/10.1179/sic.2005.50.Supplement-1.48.
[17] W.A. Badawy, M.M. Hefny, S.S. El-Egamy, Effect of Some Organic Amines as Corrosion Inhibitors for Lead in 0.3 M HCl Solution, CORROSION. 46 (1990) 978–982. https://doi.org/10.5006/1.3585055.
[18] B. Dus, Z. Szklarska-Smialowska, Effect of Some Phosphoroorganic Compounds on the Corrosion Rate of Various Metals in Acid Solutions, Corrosion. 28 (1972) 105–114. https://doi.org/10.5006/0010-9312-28.3.105.
[19] N.H. Helal, M.M. El-Rabiee, Gh.M.A. El-Hafez, W.A. Badawy, Environmentally safe corrosion inhibition of Pb in aqueous solutions, J. Alloys Compd. 456 (2008) 372–378. https://doi.org/10.1016/j.jallcom.2007.02.087.
[20] A. Adriaens, F. De Bisschop, M. Dowsett, B. Schotte, Growth and real time corrosion resistance monitoring of lead decanoate coatings, Appl. Surf. Sci. 254 (2008) 7351–7355. https://doi.org/10.1016/j.apsusc.2008.05.333.
[21] M. Dowsett, A. Adriaens, B. Schotte, G. Jones, L. Bouchenoire, *In-situ* spectroelectrochemical study of the growth process of a lead decanoate coating as

corrosion inhibitor for lead surfaces, Surf. Interface Anal. 41 (2009) 565–572. https://doi.org/10.1002/sia.3062.
[22] W. Qafsaoui, A.E. Taouil, M.W. Kendig, H. Cachet, S. Joiret, H. Perrot, H. Takenouti, Coupling of electrochemical, electrogravimetric and surface analysis techniques to study dithiocarbamate/bronze interactions in chloride media, Corros. Sci. 130 (2018) 190–202. https://doi.org/10.1016/j.corsci.2017.10.034.
[23] W. Qafsaoui, A. Et Taouil, M.W. Kendig, O. Heintz, H. Cachet, S. Joiret, H. Takenouti, Corrosion protection of bronze using 2,5-dimercapto-1,3,4-thiadiazole as organic inhibitor: spectroscopic and electrochemical investigations, J. Appl. Electrochem. 49 (2019) 823–837. https://doi.org/10.1007/s10800-019-01329-8.
[24] M. Pourbaix, Atlas of electrochemical equilibria in aqueous solutions / by Marcel Pourbaix; trans. from the French by James A. Franklin (except sections I, III 5 and III 6, which were originally written in English), 2nd ed., National Association of Corrosion Engineers, Houston, 1974.
[25] A.M. Beccaria, E.D. Mor, G. Bruno, G. Poggi, Investigation on lead corrosion products in sea water and in neutral saline solutions, Mater. Corros. Korros. 33 (1982) 416–420. https://doi.org/10.1002/maco.19820330707.
[26] R.J. Thibeau, C.W. Brown, A.Z. Goldfarb, R.H. Heidersbach, Infrared and Raman Spectroscopy of Aqueous Corrosion Films on Lead, J. Electrochem. Soc. 127 (1980) 37–44. https://doi.org/10.1149/1.2129635.
[27] K.J. Powell, P.L. Brown, R.H. Byrne, T. Gajda, G. Hefter, A.-K. Leuz, S. Sjöberg, H. Wanner, Chemical speciation of environmentally significant metals with inorganic ligands. Part 3: The Pb2+ + OH–, Cl–, CO32–, SO42–, and PO43– systems (IUPAC Technical Report), Pure Appl. Chem. 81 (2009) 2425–2476. https://doi.org/10.1351/PAC-REP-09-03-05.
[28] W. Qafsaoui, M.W. Kendig, H. Perrot, H. Takenouti, Coupling of electrochemical techniques to study copper corrosion inhibition in 0.5molL−1 NaCl by 1-pyrrolidine dithiocarbamate, Electrochimica Acta. 87 (2013) 348–360. https://doi.org/10.1016/j.electacta.2012.09.056.
[29] W. Qafsaoui, M.W. Kendig, S. Joiret, H. Perrot, H. Takenouti, Ammonium pyrrolidine dithiocarbamate adsorption on copper surface in neutral chloride media, Corros. Sci. 106 (2016) 96–107. https://doi.org/10.1016/j.corsci.2016.01.029.
[30] Z. Ghasemi, A. Tizpar, The inhibition effect of some amino acids towards Pb–Sb–Se–As alloy corrosion in sulfuric acid solution, Appl. Surf. Sci. 252 (2006) 3667–3672. https://doi.org/10.1016/j.apsusc.2005.05.043.
[31] A. Tizpar, Z. Ghasemi, The corrosion inhibition and gas evolution studies of some surfactants and citric acid on lead alloy in 12.5M H2SO4 solution, Appl. Surf. Sci. 252 (2006) 8630–8634. https://doi.org/10.1016/j.apsusc.2005.11.084.
[32] M.H. Brooker, S. Sunder, P. Taylor, V.J. Lopata, Infrared and Raman spectra and X-ray diffraction studies of solid lead(II) carbonates, Can. J. Chem. 61 (1983) 494–502. https://doi.org/10.1139/v83-087.
[33] E. Sathiyaraj, S. Thirumaran, Synthesis and spectral studies on Pb(II) dithiocarbamate complexes containing benzyl and furfuryl groups and their use as precursors for PbS nanoparticles, Spectrochim. Acta. A. Mol. Biomol. Spectrosc. 97 (2012) 575–581. https://doi.org/10.1016/j.saa.2012.06.052.
[34] G.D. Thorn, ABSORPTION SPECTRA OF 2,5-DIMERCAPTO-1,3,4-THIADIAZOLE AND ITS METHYL DERIVATIVES, Can. J. Chem. 38 (1960) 1439–1444. https://doi.org/10.1139/v60-202.
[35] https://spectrabase.com/spectrum/FX83QBXPz4u, (n.d.).

[36] V. Flexer, R. Grayburn, M. de Keersmaecker, E.A.A. Mohammed, M.G. Dowsett, A. Adriaens, A New Strategy for Corrosion Inhibition Coatings for Lead Heritage Metal Objects, Electrochimica Acta. 179 (2015) 441–451. https://doi.org/10.1016/j.electacta.2015.05.022.
[37] O. Gharbi, M.T.T. Tran, M.E. Orazem, B. Tribollet, M. Turmine, V. Vivier, Impedance Response of a Thin Film on an Electrode: Deciphering the Influence of the Double Layer Capacitance, ChemPhysChem. 22 (2021) 1371–1378. https://doi.org/10.1002/cphc.202100177.
[38] B. Hirschorn, M.E. Orazem, B. Tribollet, V. Vivier, I. Frateur, M. Musiani, Determination of effective capacitance and film thickness from constant-phase-element parameters, Electrochimica Acta. 55 (2010) 6218–6227. https://doi.org/10.1016/j.electacta.2009.10.065.
[39] B. Hirschorn, M.E. Orazem, B. Tribollet, V. Vivier, I. Frateur, M. Musiani, Constant-Phase-Element Behavior Caused by Resistivity Distributions in Films, J. Electrochem. Soc. 157 (2010) C458. https://doi.org/10.1149/1.3499565.
[40] M. Benoit, C. Bataillon, B. Gwinner, F. Miserque, M.E. Orazem, C.M. Sánchez-Sánchez, B. Tribollet, V. Vivier, Comparison of different methods for measuring the passive film thickness on metals, Electrochimica Acta. 201 (2016) 340–347. https://doi.org/10.1016/j.electacta.2015.12.173.
[41] Rumble Jr, John R, M.J. Doa, T.J. Bruno, CRC handbook of chemistry and physics: a ready-reference book of chemical and physical data, 2020.
[42] L. Young, Anodic oxide films. Part 4.—The interpretation of impedance measurements on oxide coated electrodes on niobium, Trans Faraday Soc. 51 (1955) 1250–1260. https://doi.org/10.1039/TF9555101250.
[43] H. Göhr, J. Schaller, C.-A. Schiller, Impedance studies of the oxide layer on zircaloy after previous oxidation in water vapour at 400°C, Electrochimica Acta. 38 (1993) 1961–1964. https://doi.org/10.1016/0013-4686(93)80323-R.
[44] M.E. Orazem, B. Tribollet, Electrochemical Impedance Spectroscopy: Orazem/Electrochemical, John Wiley & Sons, Inc., Hoboken, NJ, USA, 2008. https://doi.org/10.1002/9780470381588.
[45] E. Ngaboyamahina, H. Cachet, A. Pailleret, E.M.M. Sutter, Electrochemical impedance spectroscopy characterization of conducting polymer/TiO2 nanotube array hybrid structures, J. Electroanal. Chem. 737 (2015) 37–45. https://doi.org/10.1016/j.jelechem.2014.09.029.

Table 1. Corrosion parameters of Pb electrode after one hour immersion in 30 g L^{-1} NaCl without (Blank) or with 10 mM PDTC or 10 mM DMTD.

	E_{corr} (mV vs. SCE)	**j_{corr} (A /cm²)**	**τ (%)**
Blank	-575 (± 10)	5.0 (± 0.2) 10^{-7}	_
10 mM DMTD	-402 (± 10)	6.0 (± 0.2) 10^{-8}	88 (± 1)
10 mM PDTC	-580 (± 10)	5.0 (± 0.2) 10^{-8}	90 (± 1)

Table 2. Effect of the film impedance representation (CPE, Young or PL models) on the estimated values of the interfacial parameters defined according to the electrical scheme given in Fig.7. (For each parameter and system, the mean values are calculated as the average of the corresponding values for the three models. The last column indicates the fit quality, a value of 1 meaning that the adjustment lies within a 1% error on impedance data. These selected data correspond to a 12-hour immersion).

Parameters → / **↓ System model ↓**		**C_{dl}** **µF/cm²**	**R_f** **Ω.cm²**	**R_{tc}** **Ω.cm²**	**W_c** **Ω.s$^{-1/2}$**	**R_{ta}** **Ω.cm²**	**W_a** **Ω.s$^{-1/2}$**	**R_s** **Ω.cm²**	**Fit standard deviation**
BlankPb	CPE	1.00 ±0.30	4.5 ±2	1270 ±60	15150 ±250	12150 ±170	306 ±50	4.4 ±0.1	1.78
	Young	0.94 ±0.08	5.3 ±2.7	1360 ±140	15300 ±610	12140 ±400	304 ±170	4.45 ±0.15	1.21
	Power law	0.81 ±0.07	7 ±6	1250 ±120	15040 ±550	12160 ±370	300 ±165	4.4 ±0.3	1.28
	Mean value	0.92 ±0.10	5.8 ±1.7	1300 ±60	15200 ±130	12150 ±10	303 ±3	4.42 ±0.03	
Pb/DMTD	CPE	0.085 ±0.014	6780 ±930		31300 ±3100	236000 ±2800	7700 ±640	4.4 ±0.1	1.02
	Young	0.070 ±0.030	6540 ±1130		321700 ±10000	234500 ±6000	8220 ±8220	4.44 ±0.10	1.06
	Power law	0.085 ±0.016	6810 ±1050		309000 ±9000	239000 ±4500	8090 ±1900	4.3 ±0.5	0.70
	Mean value	0.080 ±0.009	6700 ±150		315000 ±6500	236500 ±2300	8000 ±270	4.4 ±0.1	
Pb/PDTC	CPE	0.018 ±0.004	10400 ±2400		$1.10\ 10^6$ ±16500	511400 ±7200	34500 ±1900	4.4 ±0.1	1.53
	Young	0.014 ±0.007	10100 ±3500		$1.09\ 10^6$ ±46000	508400 ±14000	34900 ±6600	4.4 ±0.4	0.73
	Power law	0.011 ±0.007	13040 ±3900		$1.09\ 10^6$ ±46500	506400 ±14000	35600 ±6650	4.3 ±3.6	1.13
	Mean value	0.014 ±0.004	11200 ±1600		$1.09\ 10^6$ ±6000	509000 ±2500	35000 ±600	4.4 ±0.1	

Figures

Fig. 1. Structures of ammonium pyrrolidinedithiocarbamate (PDTC) (a) and 2,5-dimercapto-1,3,4-thiadiazole (DMTD) (b).

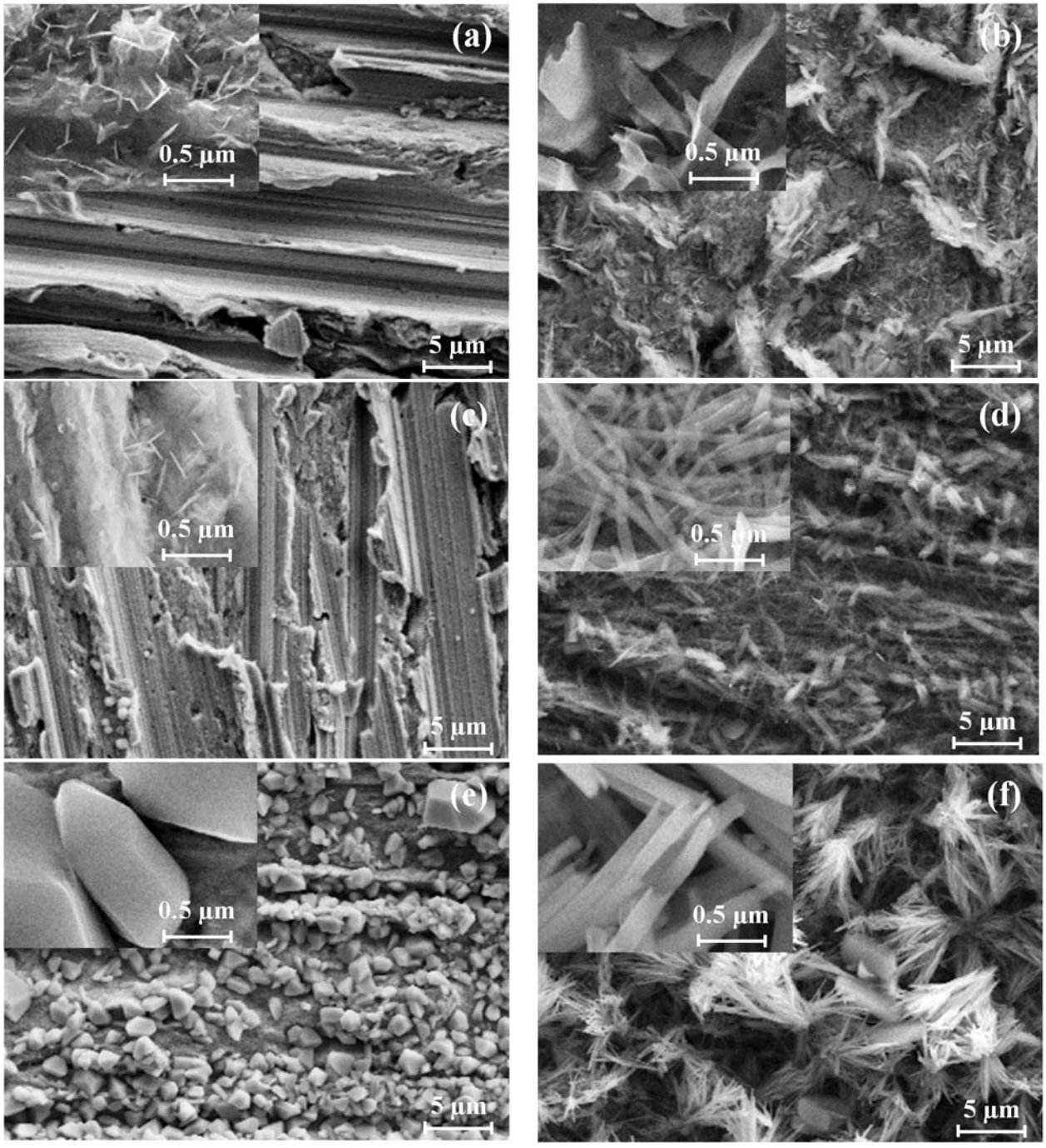

Fig. 2. SEM images of Pb bare surface (a) and after 24 h immersion in 30 g L^{-1} NaCl without (b) or with 0.1 mM PDTC (c), 10 mM PDTC (d), 0.1 mM DMTD (e),10 mM DMTD (f).

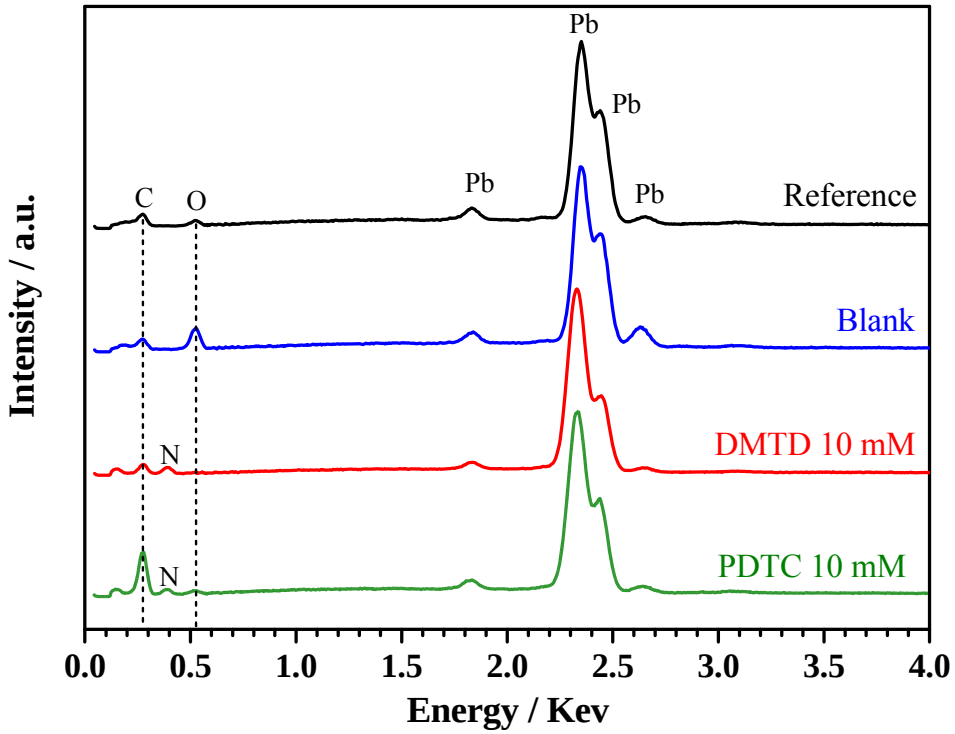

Fig. 3. EDX analysis of Pb bare surface (reference) and after 24 h immersion in 30 g L^{-1} NaCl without and with 10 mM PDTC or 10 mM DMTD.

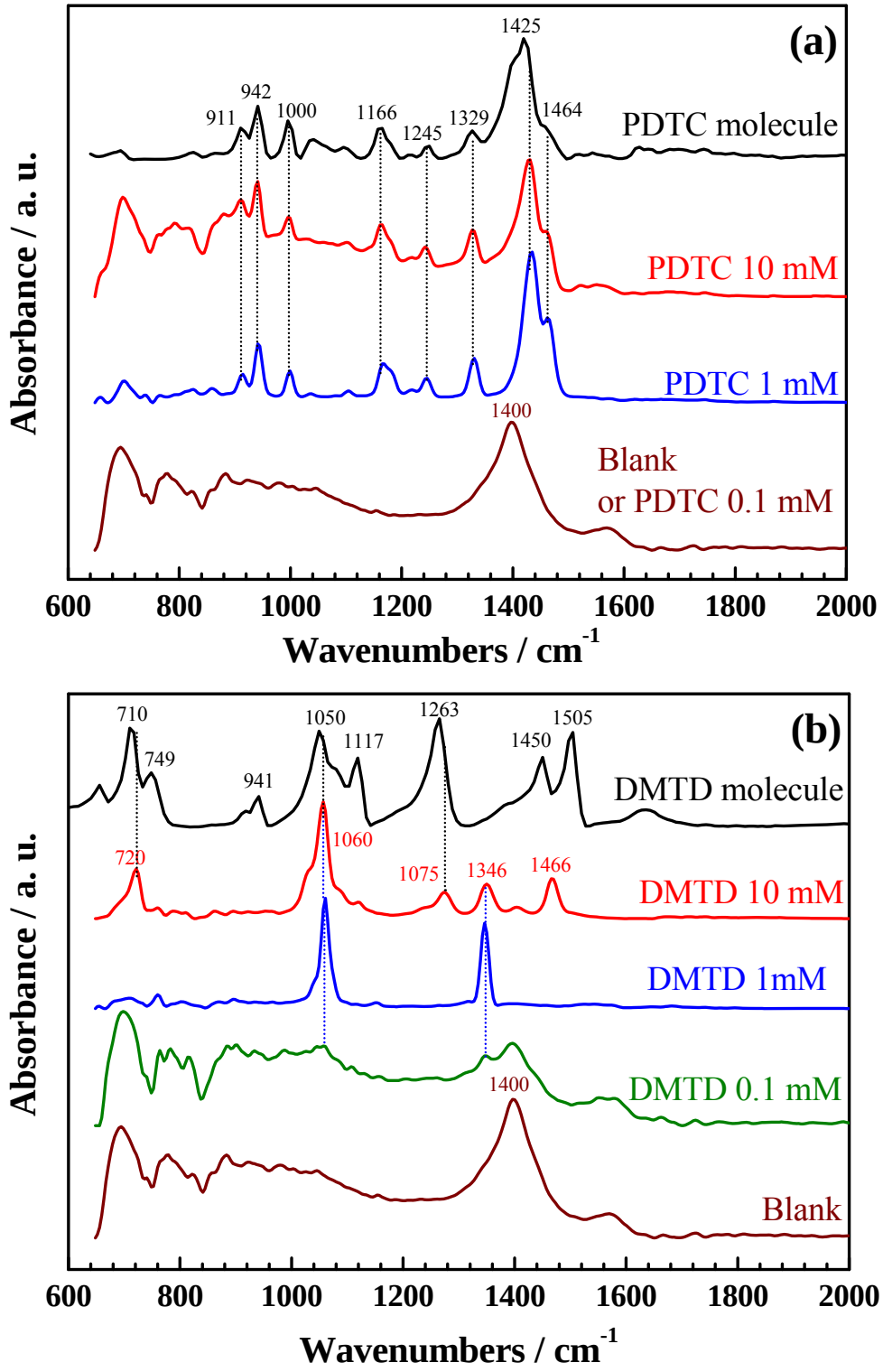

Fig. 4. FT-IR spectra collected from PDTC molecule and from Pb electrode after 24 h immersion in 30 g L^{-1} NaCl without (Blank) or with 0.1 mM, 1 mM or 10 mMPDTC (a) and from DMTD molecule and from Pb electrode after 24 h immersion in 30 g L^{-1} NaCl without (Blank) or with 0.1 mM, 1mM or 10 mM DMTD (b).

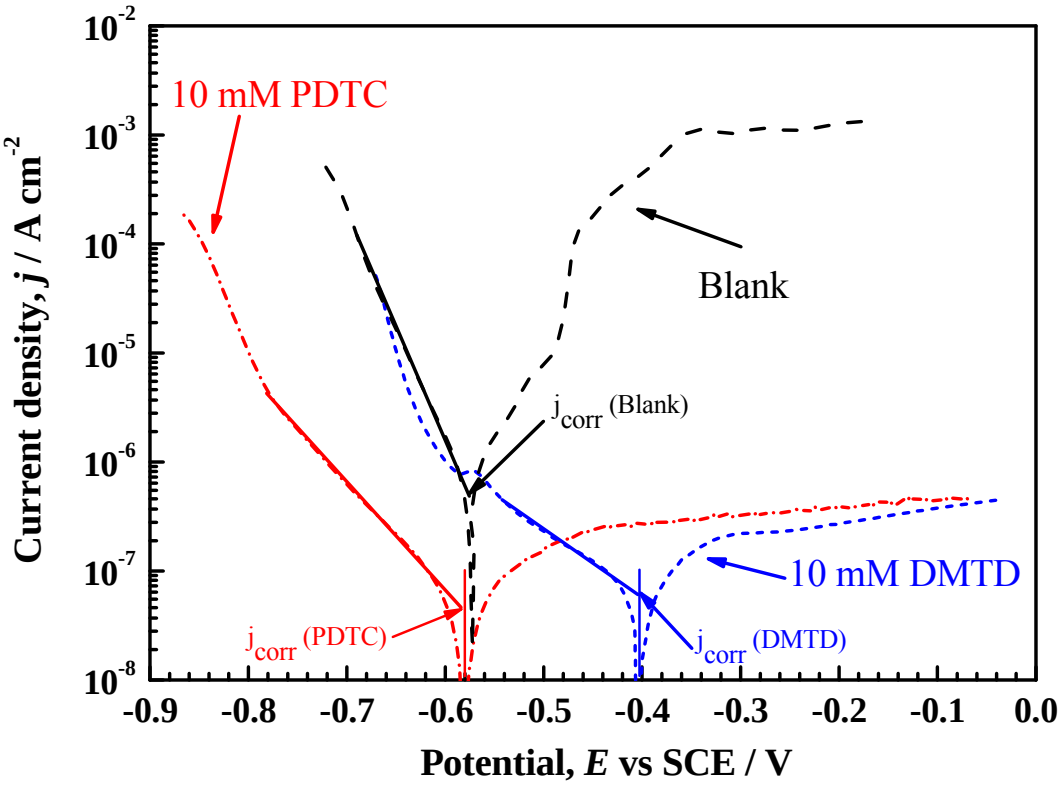

Fig. 5. Polarization curves at 1 mV s^{-1} for Pb electrode after one hour immersion in 30 g L^{-1} NaCl without (Blank) or with 10 mM PDTC or 10 mM DMTD.

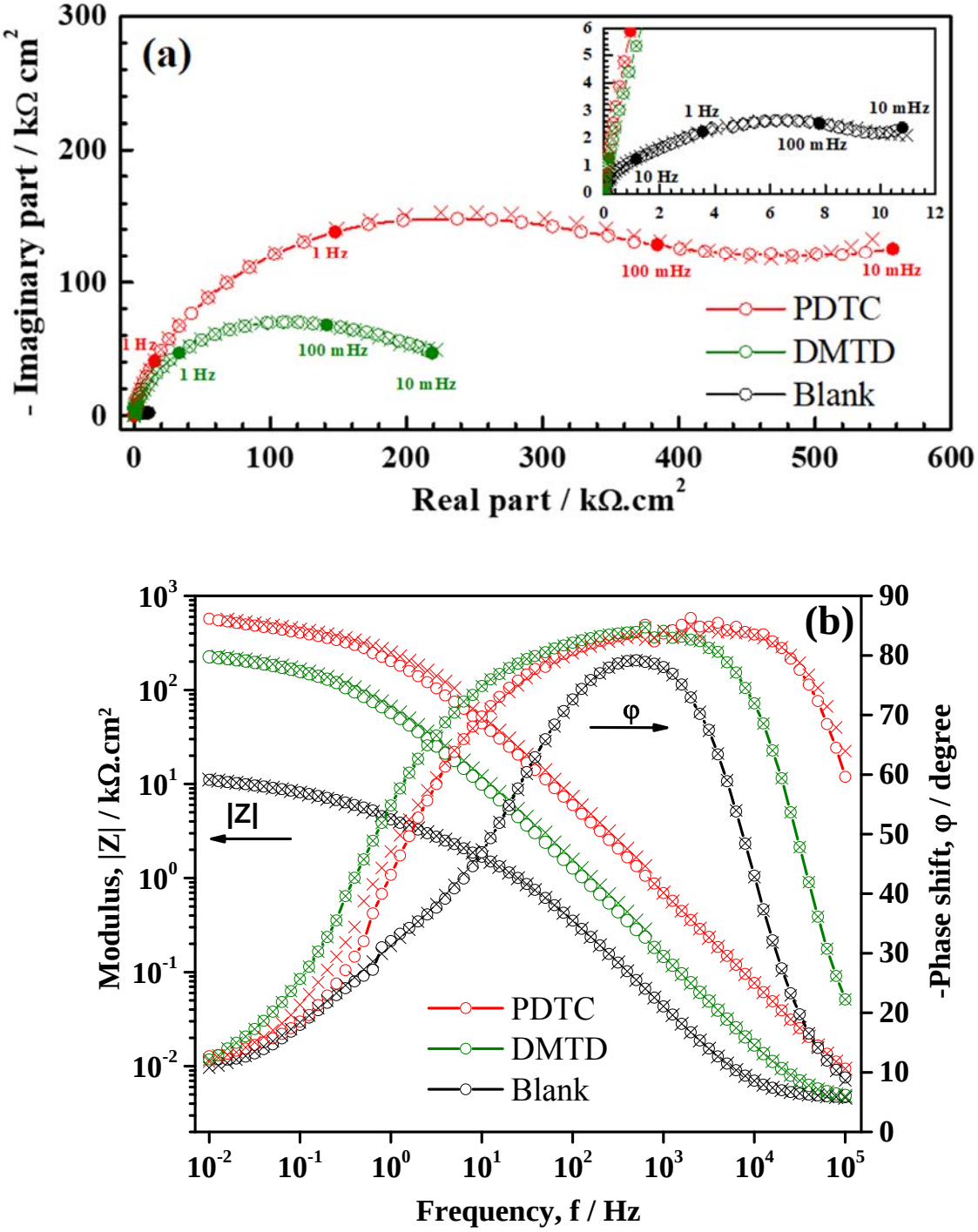

Fig. 6. Nyquist (a) and Bode (b) diagrams of Pb electrode after 12 hours immersion in 30 g L^{-1} NaCl without (Blank) or with 10 mM PDTC or 10 mM DMTD; stationary electrode at 20 °C.

The insert shows an expanded view of the blank diagram.

Symbols: (○) experimental data and (□) calculated data.

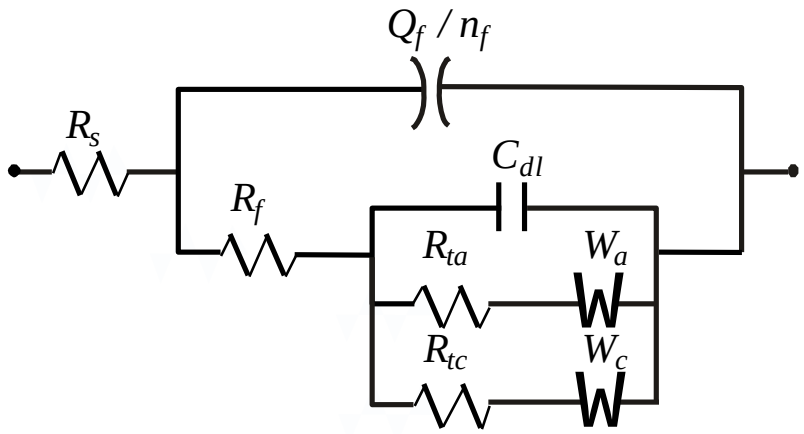

Fig. 7. Electrical equivalent circuit to reproduce experimental impedance spectra for Pb electrode in 30 g L^{-1} NaCl without or with PDTC or DMTD.

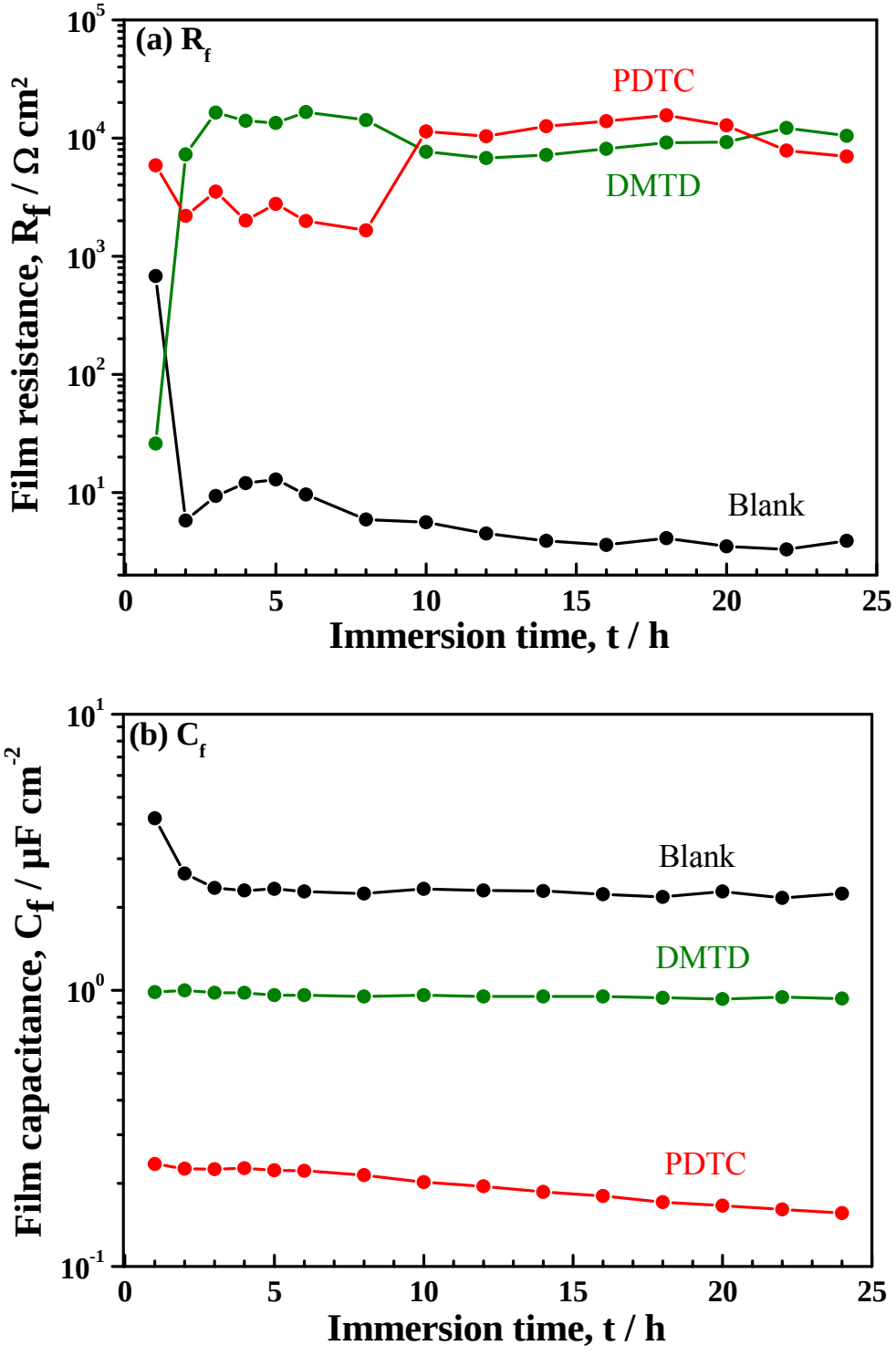

Fig. 8. R_f (a) and C_f (b) changes as a function of immersion time for Pb in 30 g L^{-1} NaCl without (Blank) or with 10 mM PDTC or 10 mM DMTD; stationary electrode at 20 °C.

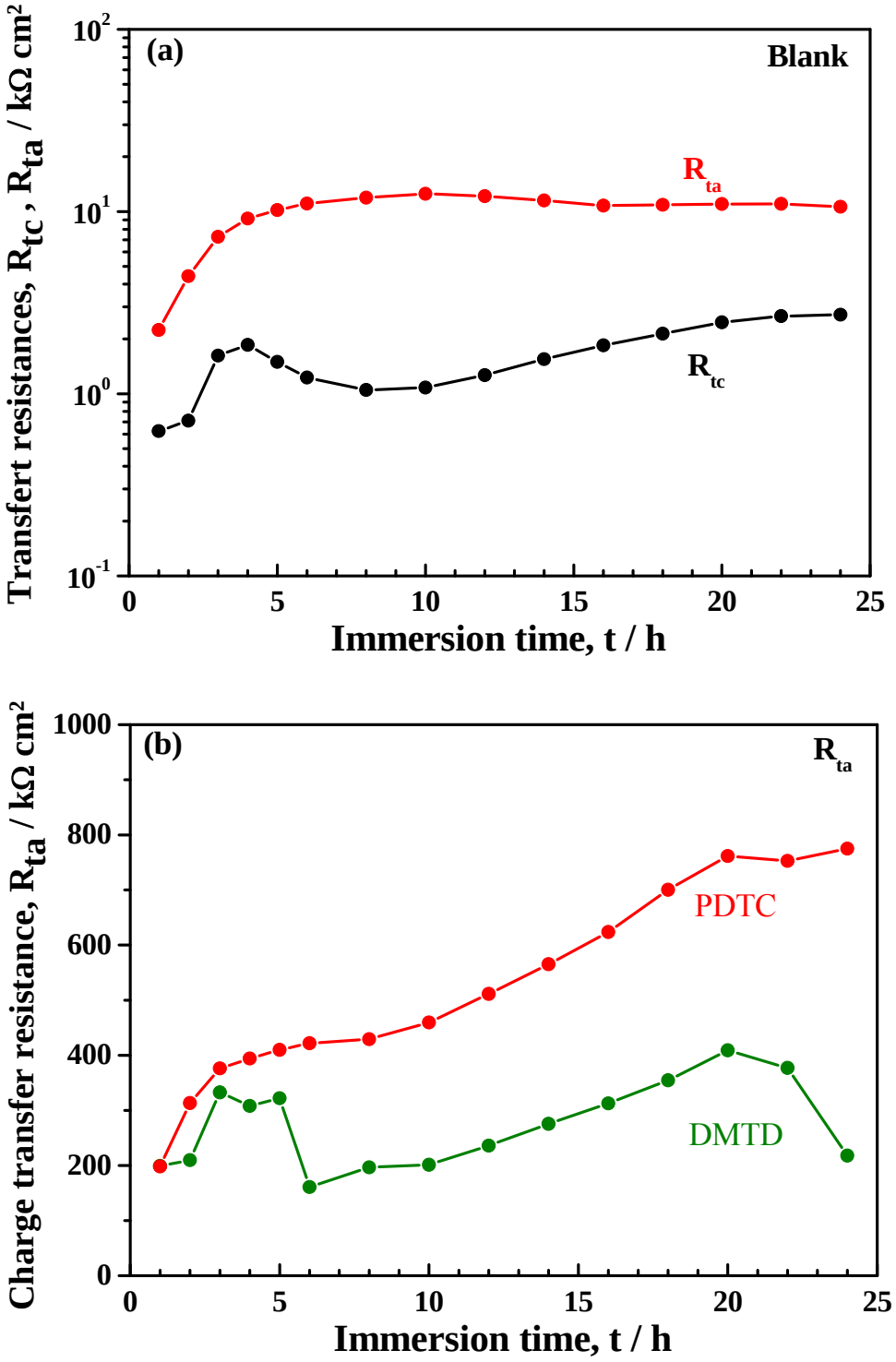

Fig. 9. R_{ta} and R_{tc} changes as a function of immersion time for Pb in 30 g L^{-1} NaCl (a) and R_{ta} changes as a function of immersion time for Pb in 30 g L^{-1} NaCl with 10 mM PDTC or 10 mM DMTD (b) ; stationary electrode at 20 °C.

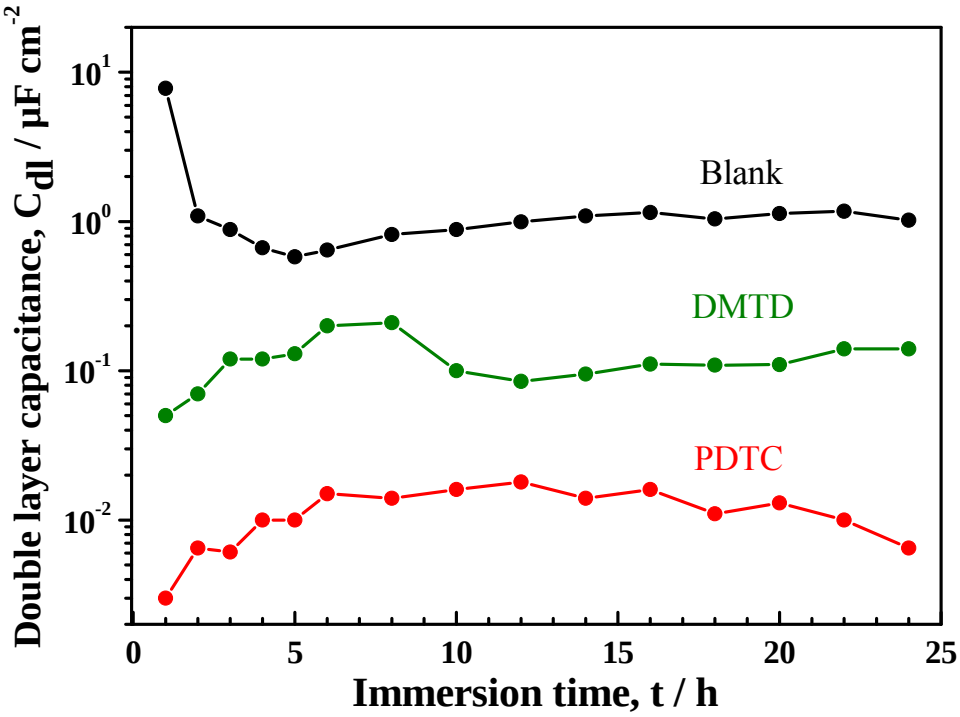

Fig. 10. C_{dl} changes as a function of immersion time for Pb in 30 g L^{-1} NaCl without (Blank) or with 10 mM PDTC or 10 mM DMTD; stationary electrode at 20 °C.

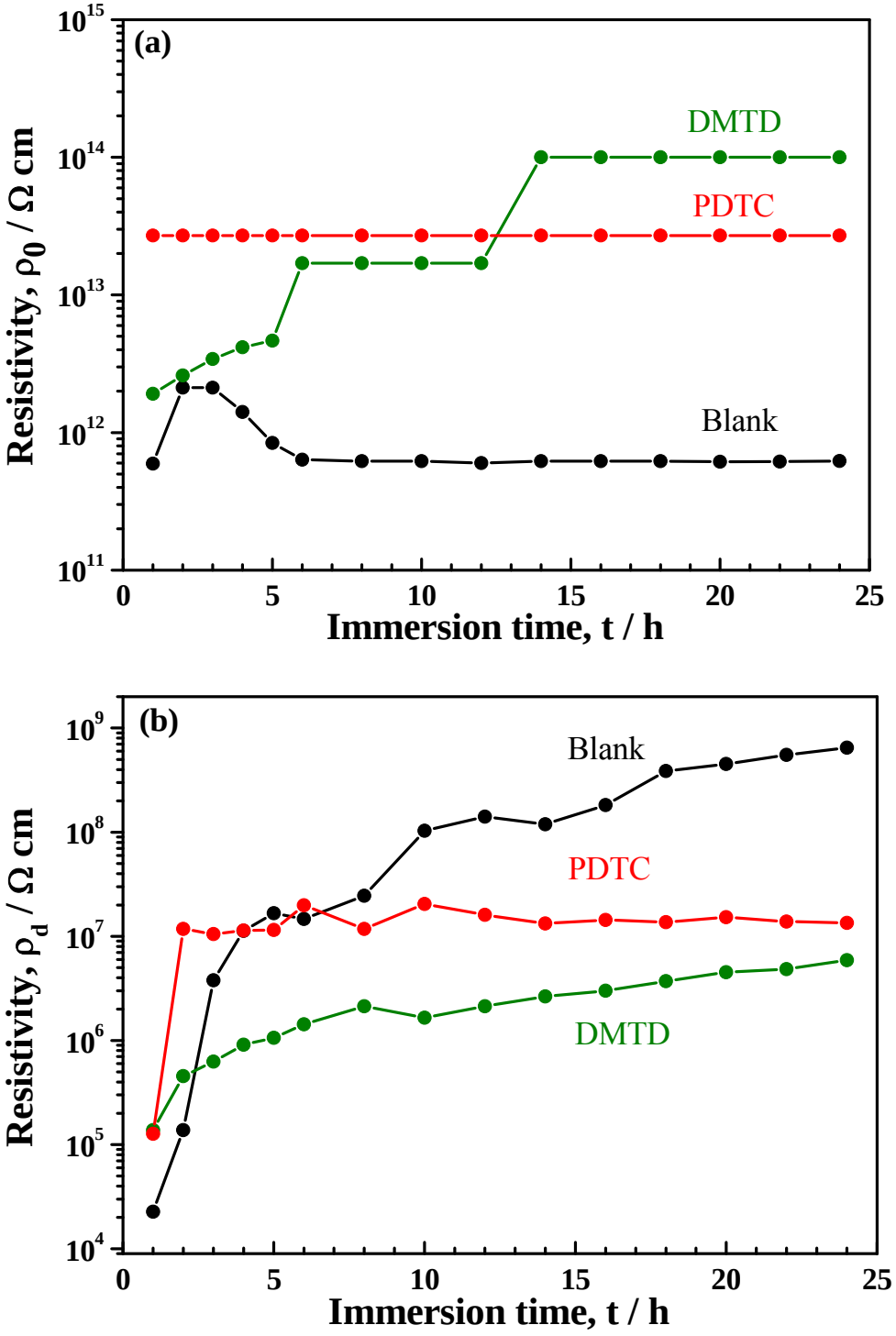

Fig. 11. Changes of the resistivity ρ_0 at the metal/surface film interface (a) and the resistivity ρ_d at the surface film /solution interface (b) as a function of immersion time for Pb in 30 g L^{-1} NaCl without (Blank) or with 10 mM PDTC or 10 mM DMTD.